THE SEISMOLOGICAL SOCIETY OF AMERICA
400 Evelyn Ave., Suite 201
Albany, CA 94706-1375
(510) 525-5474; FAX (510) 525-7204
www.seismosoc.org

Determination of Site Amplification from Regional Seismicity: Application to the Swiss National Seismic Networks

by Benjamin Edwards, Clotaire Michel, Valerio Poggi, and Donat Fäh

Online Material: Supplemental figures and tables.

INTRODUCTION

The propagation of energy released by an earthquake through the uppermost crust has a significant impact on the ground motion that is observed at the surface. Knowledge of this site amplification effect can significantly reduce the uncertainty involved in the determination and application of stochastic or empirical predictive ground-motion equations and therefore reduce the uncertainty in subsequent hazard calculations. However, due to the heterogeneity of the upper crust, the site amplification effect is highly variable over scales of kilometers or less (e.g., Boore, 2004).

It is important to characterize site amplification at seismic instrument locations in order to correct or account for data from several recording sites, such that a common reference (e.g., Poggi *et al.*, 2011) is defined in ground-motion prediction equations (GMPEs). State of the art GMPEs take advantage of site characterization based on broad classes, such as National Earthquake Hazards Reduction Program (NEHRP) soil class (BSSC, 2003; Akkar and Bommer, 2010), or the average shear-wave velocity of the uppermost 30 m (V_{S30}; e.g., Abrahamson and Silva, 2008). However, despite the use of this simple characterization, recent work has shown the importance of considering site-to-site amplification variability in the estimation of ground-motion prediction uncertainty (Atkinson, 2006; Al Atik *et al.*, 2010). This highlights that the strong variability of site amplification, even within a single NEHRP or V_{S30} class, contributes significantly to the uncertainty of ground-motion prediction.

Developers of GMPEs typically make an assumption of ergodicity; that is, that the variability over space is treated as an uncertainty in time. Spatial variability (beyond simple site classification) is therefore assumed to be zero. In order to minimize the influence of site-to-site variability in single-site hazard analyses, Atkinson (2006) introduced the concept of single-site sigma (uncertainty). Its use can lead to reduced site-specific hazard due to the fact that, contrary to the ergodic assumption, the uncertainty of ground motion observed at a single site is lower than that over a range of sites. The single-site sigma approach is particularly applicable in seismic hazard analyses of sensitive facilities due to the fact that, in such cases, extensive site characterization studies are undertaken. Given such knowledge, the site-to-site component of uncertainty buried in the sigma of GMPEs is clearly superfluous.

One approach taken to isolate the influence of site-to-site variability in GMPE development, and subsequently obtain single-site sigma, is through direct regression, or, alternatively, residual analysis (e.g., Al Atik *et al.*, 2010). However, statistical analyses, particularly of small datasets coupled with GMPEs with high degrees of freedom, are sensitive to trade-off problems. Furthermore, the site-of-interest may not share the characteristics of any of the recording sites used to construct the GMPE. This makes it difficult to assign a particular single-site sigma to the hazard analysis. A more thorough approach, which we explore in this article, is to consider the site amplification at recording instrumentation sites based on the physical properties of the site (e.g., the measured velocity profile). Given such information, we facilitate a uniquely referenced site-specific GMPE that could easily be adapted to an arbitrary target site for hazard analysis.

Of course, there is reasoning behind the use of simple site characterization approaches in GMPE development; typically, even basic V_{S30} characterization may not exist for a given site. One potential candidate for site-specific amplification determination is the horizontal to vertical (H/V) spectral ratio. H/V spectral ratios extracted from ambient vibrations have been proposed as a simple easy-to-derive proxy for site amplification (e.g., Nakamura, 1989; Atkinson and Boore, 2006). However, other authors (e.g., Scherbaum *et al.*, 2003; Bonnefoy-Claudet *et al.*, 2006) have showed the limitations and incorrectness of its use; while it can be shown that the frequencies at which resonance occurs, for instance due to strong impedance contrasts at depth (Fäh *et al.*, 2001), the amplitude of H/V ratios are not representative of ground-motion amplification. This is simply because the vertical component of motion itself undergoes unknown amplification and cannot therefore be considered a suitable reference.

doi: 10.1785/0220120176

Often 1D modeling is used to compute the theoretical elastic SH-transfer function (SHTF) based on known or inferred shear wave velocity profiles (e.g., Fäh *et al.*, 2003; Poggi *et al.*, 2012). However, obtaining a detailed estimate of the velocity profile to a sufficient depth for such computations might be impractical due to high implementation costs in the case of borehole logging or high-resolution active seismic techniques. Even when low-cost, non-invasive measurement techniques such as array analysis of the natural ambient vibration wavefield are used (e.g., Fäh *et al.*, 2008; Poggi and Fäh, 2010), problems exist. For such measurements, sites with smooth topography and low lateral variability over an area comparable to the expected penetration depth are required in order to acquire data that allows for the reconstruction of the velocity profile. This may not be possible, particularly in regions of complex or laterally heterogeneous geology, such as at the edge of sedimentary basins. When high quality 1D shear-wave velocity profiles are available, 1D site amplification modeling methods do not consider the lateral complexity of the near surface and topography and therefore neglect 2D and 3D amplification effects often observed in Alpine valleys (e.g., Roten *et al.*, 2008; Thompson *et al.*, 2012). Finally, in the case of anelastic SHTF, uncertainties are particularly high due to the uncertainty of attenuation information, with Q typically estimated based on geology.

The standard spectral ratio (SSR) method (Borcherdt, 1970) has, for many years, been considered the only reliable technique to derive site amplification that include such effects. However, it assumes the absence of local effects at the reference site and that the same rock profile can be found below the reference and the target site. Moreover, SSR refers to a rock reference that is relevant only at the local scale, with the variations in the local rock reference properties from V_{S30} around 700–2500 m/s. Finally, the cost of installing an additional reference station to a strong-motion station on soil is high, and often no rock outcrop is available close to the site of interest.

In this article we present an alternative method through empirical spectral modeling (ESM) that can be used to obtain site amplification at instrument locations of a permanent or temporary seismic network given sufficient recordings of small or moderate earthquakes. In practice the method is a combination of physical modeling and statistical approach. The methodology is based on an established approach of separating source, path, and site effects, for example, through a generalized inversion (Field and Jacob, 1995). In our implementation, we compare recorded seismograms' spectra with those expected from a Brune (1970, 1971) ω^2 source model, accounting for geometrical decay and path attenuation (Edwards *et al.*, 2008; Edwards and Fäh, 2013) on an event-by-event basis. Subsequent determination of magnitude following Edwards *et al.* (2010) and residual analysis for consistent site effects over all recorded events facilitates the determination of referenced amplification. Each new event is processed individually, with the resulting event-specific amplification added to the statistical representation of the database site-response functions, leading to increasingly robust results with time. This allows us to avoid both the limitations of the simple 1D amplification function, and the limitations of non-physical parametric analysis (as in the case of most GMPEs).

The proposed technique is employed within the routine monitoring of the Swiss Seismological Service (SED). The SED produces automatic hypocenter determination solutions of regional seismicity, with a magnitude (M_L) of completeness of at least 2.0 over the entire Switzerland. These hypocenter solutions are used to trigger the automatic creation or update of a site-response function database for all stations with continuous recording within the networks operated by the SED. A web interface is employed to allow for visualization and interpretation, providing an illustration of amplification phenomena immediately after the earthquake is recorded. This proves particularly useful in the case of newly installed sites relating to the rapidly expanding Swiss Strong-Motion Network (Clinton *et al.*, 2011).

In order to test our approach we show a number of examples of empirical amplification and compare it to site-to-reference spectral ratios (SSR), 1D SH-wave modeling and single station H/V of ambient vibration recordings. Comparisons account for reference corrections in order to cope with the limitations of locally referenced methods.

EARTHQUAKE RECORDINGS

The expanding earthquake waveform database of the SED was used as a basis for our work. This comprises the broadband Swiss Digital Seismic Network (SDSNet; Deichmann *et al.*, 2010) and the Swiss Strong Motion Network (SSMNet; Clinton *et al.*, 2011). We use recordings starting from January 2010. Automated trace-windowing and quality control of the resulting spectra are performed following Edwards *et al.* (2010) to ensure only reliable data are included in this inversion; the minimum and maximum frequencies considered are 0.1–30 Hz, although the included bandwidth of individual spectra depends on the relative noise level. Our analysis window comprises the 5%–95% energy integral around the direct *S* wave and coda. The noise estimate, taken from the waveform prior to the *P*-wave arrival, is artificially increased until it intersects the signal spectrum at its lowest and highest frequencies. The conservative noise estimation prevents subsequent modeling being influenced by the noise, and is reasonable for small to moderate earthquakes, as at very low or high frequencies the signal is typically dominated by background noise. Finally, the maximum bandwidth over which the signal is at least three times greater than the noise is selected. If the frequency range covers at least an order of magnitude, the record is retained and, given three or more stations per event fulfilling the quality check, the data are passed through to the inversion stage.

SITE AMPLIFICATION FROM BROADBAND SPECTRAL FITTING

Given instrument corrected data, the Fourier velocity spectrum Ω_{ij}, observed at a station j originating from an earthquake i is represented by

$$\Omega_{ij}(f,r) = 2\pi f E_i(f, M_{0i}, f_{ci}) B_{ij}(f, t^*_{ij}) S_{ij}(r, r_{0\ldots n-1}, \lambda_{1\ldots n}) \times T_j(f, A_j, \Delta\kappa_j) T_{\mathrm{Ref}}(f, A_{\mathrm{Ref}}, \kappa_{\mathrm{Ref}}), \quad (1)$$

for which f is the frequency, r is the hypocentral distance, $E_i(f, M_{0i}, f_{ci})$ is the source model, $B_{ij}(f, t^*_{ij})$ is the intrinsic attenuation along the ray path, $S_{ij}(r, r_{0\ldots n-1}, \lambda_{1\ldots n})$ is the frequency independent amplitude decay with distance, and $T_j(f, A_j, \Delta\kappa_j)$ is the site-response function at the station relative to the reference $T_{\mathrm{Ref}}(f, A_{\mathrm{Ref}}, \kappa_{\mathrm{Ref}})$ with $A_{\mathrm{Ref}} = 1$. The source spectrum E_i, is a Brune (1970, 1971) ω^2 spectrum with event-specific corner frequency f_c and long-period spectral plateau defined by the seismic moment, M_{0i}. B_{ij} is given by the model according to Anderson and Hough (1984), with path attenuation operator t^*.

The geometrical spreading function S_{ij}, is described by a piecewise function comprising two segments of constant exponential decay in the form $R^{-\lambda}$: initial spherical decay ($\lambda_1 = 1.0$) followed by trapped surface wave (cylindrical, $\lambda_2 = 0.5$) spreading after $r_1 = 150$ km (Atkinson and Mereu, 1992). Finally, local site amplification, relative to a regional reference (including local attenuation) is given by

$$T_j(f) = A_j a_j(f) e^{-\pi f \Delta\kappa_j}, \quad (2)$$

for which A_j is the average site amplification (the average amplification over all frequencies), $\Delta\kappa_j$ is a constant, site-related attenuation operator (Anderson and Hough, 1984) and $a_j(f)$ is the frequency-dependent site amplification function. The relative site attenuation operator $\Delta\kappa_j$ is related to absolute site attenuation κ_j by

$$\Delta\kappa_j = \kappa_j - \kappa_{\mathrm{Ref}}, \quad (3)$$

for which κ_{Ref} is the local attenuation of the reference site.

A modification of the method of Edwards *et al.* (2008, 2010) is followed to deconvolve equation (1) for a single earthquake. We first determine the combined path attenuation term at each site $t^*_j + \kappa_j$, the event-common source corner frequency f_c, and a spectral amplitude parameter termed the signal moment for each spectrum. Here we do not define a regional attenuation model to pre-determine $t^*_j + \kappa_j$ because this requires simultaneous inversion of the full dataset (rather than the event-by-event application) and may bias results due to model simplification (Edwards *et al.*, 2010). The misfit of the spectral model to the data is minimized in the log-log space with the L-2 norm. Using the resulting minimum misfit model, the residuals are then assumed to be an estimate of the frequency-dependent elastic component of the site function $a_j(f)$. If an existing estimate of this is available from previous events, the existing function is updated assuming a log-normal distribution of the estimates.

By correcting for the geometrical decay function S_j the frequency-independent component of the modeled spectra, the signal moments, can be split into a single seismic moment M_0, and average site amplification terms A_j relative to the common reference. Clearly a strong trade-off exists between the moment and average amplification. However, in Poggi *et al.* (2011), 17,300 records from 585 earthquakes occurring in Switzerland with $M_L > 2.0$ were used simultaneously to determine A_j and $a_j(f)$ for 77 instrumentation sites in Switzerland. Of these, 27 with available shear-wave velocity profiles were used to define the Swiss generic rock reference model. Our inversion is constrained by fixing the known 77 A_j values, based on the Swiss generic rock reference model, and using the corresponding $a_j(f)$ from the same study as a starting model, weighted by the number of observations used in their derivation (Edwards *et al.*, 2011; Poggi *et al.*, 2011). This enforces any subsequently derived amplification (i.e., for newly installed sites) to be defined as amplification relative to the Swiss rock reference, providing at least one recording at a station with predefined amplification is available in the inversion. The parameters defining the Fourier spectra of recordings used for the sites in this study are provided in Ⓔ Table S1. The parameters defined by Poggi *et al.* (2011) for the data prior to 2010 can be found in Ⓔ Table S2. Both Ⓔ Tables S1 and S2 can be found in the electronic supplement to this article.

For the anelastic ESM amplification function the absolute site attenuation term κ must be determined. To separate κ from the whole-path terms ($t^*_j + \kappa_j$) obtained during the spectral inversion we use the model of Edwards *et al.* (2011) to estimate the contribution from crustal attenuation t^* along the path. Because ESM amplification is with reference to a regional velocity profile, we must also account for the local attenuation at the reference using equation (3). The site attenuation at the rock reference of Poggi *et al.* (2011) was given by Edwards *et al.* (2011) as $\kappa_{\mathrm{Ref}} = 0.016$ s. Finally, the elastic or anelastic ESM amplification functions can be reconstructed from the product of A_j and $a_j(f)$ or A_j, $a_j(f)$ and $\exp(-\pi f \Delta\kappa_j)$ respectively (equation 2). An example of the elastic and anelastic ESM amplification functions is shown in Figure 1. Swiss foreland site WILA ($V_{S30} = 683$ ms^{-1}) exhibits moderate elastic amplification of up to around a factor four with respect to the reference profile ($V_{S30} = 1105$ ms^{-1}) due to its lower shear-wave velocity. On the other hand, alpine site LLS ($V_{S30} = 3011$ ms^{-1}) shows constant deamplification of around 0.4 due to shear-wave velocities much higher than those of the reference profile. For the anelastic functions, LLS shows high-frequency amplification, while WILA shows deamplification. This is due to the fact that LLS has site attenuation lower than the reference $\Delta\kappa_{\mathrm{LLS}} < 0$, and WILA has attenuation higher than at the reference profile $\Delta\kappa_{\mathrm{WILA}} > 0$.

The standard deviation of the ESM amplification functions is determined through the propagation of errors in individual components. Assuming no covariance between the parameters and given a log-normal distribution in the uncertainty of A_j and $a_j(f)$ [σ_A and $\sigma_a(f)$ respectively] and a normal distribution in $\Delta\kappa_j$ (σ_κ) we obtain the log-normal error in $T_j(f)$:

$$\sigma_T = \sqrt{\sigma_A^2 + \sigma_a^2 + \pi f \sigma_\kappa^2}. \quad (4)$$

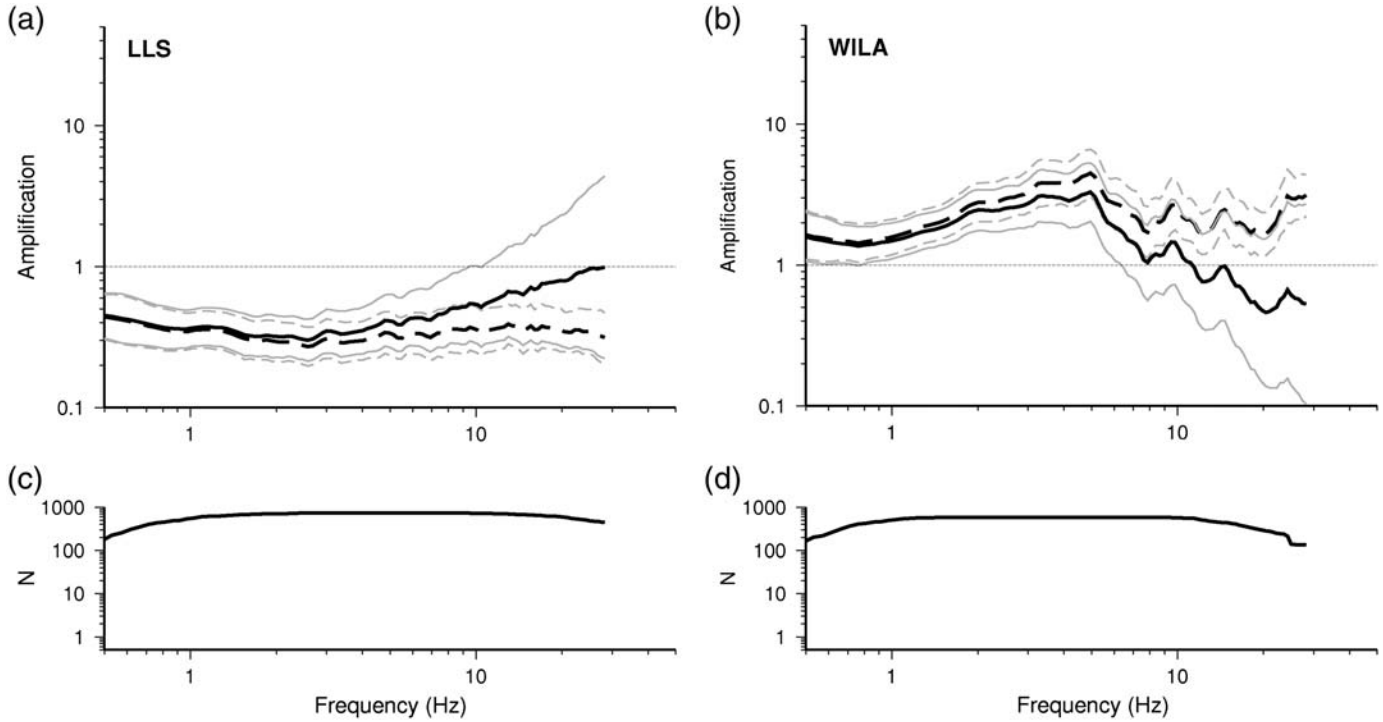

▲ **Figure 1.** Example of the dynamic ESM amplification functions displayed on the web interface for two SDSNet stations. (a) LLS, with attenuation lower than the reference. (b) WILA, with attenuation higher than the reference of 0.016 s. Solid lines show the anelastic functions, and dashed lines show the elastic functions. Black lines show mean amplification, and gray lines show standard deviation. (c) Number of records used for the determination of amplification for LLS. (d) Number of records used for the determination of amplification for WILA.

COMPARISON OF EMPIRICAL SITE AMPLIFICATION WITH SITE-TO-REFERENCE SPECTRAL RATIOS

In a first-stage validation, the proposed approach to retrieve site amplification was compared to the classical SSR approach (Borcherdt, 1970). In the SSR approach the horizontal spectra of earthquake recordings at the target site are divided by the spectra at a reference station. The reference station is typically chosen to be as close to a "non-amplifying rock site" as possible, often through the analysis of H/V spectral ratios to rule out sites exhibiting resonance. The reference station must, however, still be near to the target site in order to satisfy the assumption that source and path effects are cancelled by the spectral ratio. One such example, in the case of a target site installed in a sedimentary basin, is outcropping bedrock at the basin edge. Given a close reference and target site with respect to the recording distance, this approach has the advantage of almost completely removing any source and propagation effects through the spectral division. However, one disadvantage is that, contrary to the proposed method, the reference velocity structure as well as the attenuation is not the same for all sites (Steidl *et al.*, 1996). Furthermore, the selected local rock reference can be quite dissimilar to the expected bedrock below the target site, including some residual site effect due to weathering of the rock or shallow sediments, especially visible at high frequencies.

For the calculation of the SSR, spectra are computed for each horizontal component using the Fourier transform of *S* waves and coda, which are then smoothed following the Konno and Ohmachi (1998) procedure with a *b*-value of 80. Only the bandwidth of the spectra with sufficient signal-to-noise ratio is used (SNR larger than 3). Consistent with geometrical mean ground-motion estimation, the mean and standard deviation are computed in the log-space over all recording components available at both target and reference sites. For the ESM amplification, we use the anelastic version [the product of A_j, $a_j(f)$ and $\exp(-\pi f \Delta\kappa_j)$] as the SSR also includes relative differences in the local attenuation with respect to the reference.

Figure 2 shows a comparison of SSR amplification with that from spectral modeling for station SMUK, located in the center of the deeply filled Rhone valley, proximate to the city of Monthey. The retrieved ESM amplification of the reference station used (SMUR) shows a clear peak at 5 Hz for this "rock" site that makes a direct comparison between the ESM and SSR methods difficult. This highlights a typical, though extreme, issue with the SSR approach; the results being highly dependent on having a non-amplifying local reference site. In order to make a meaningful comparison, rather than directly

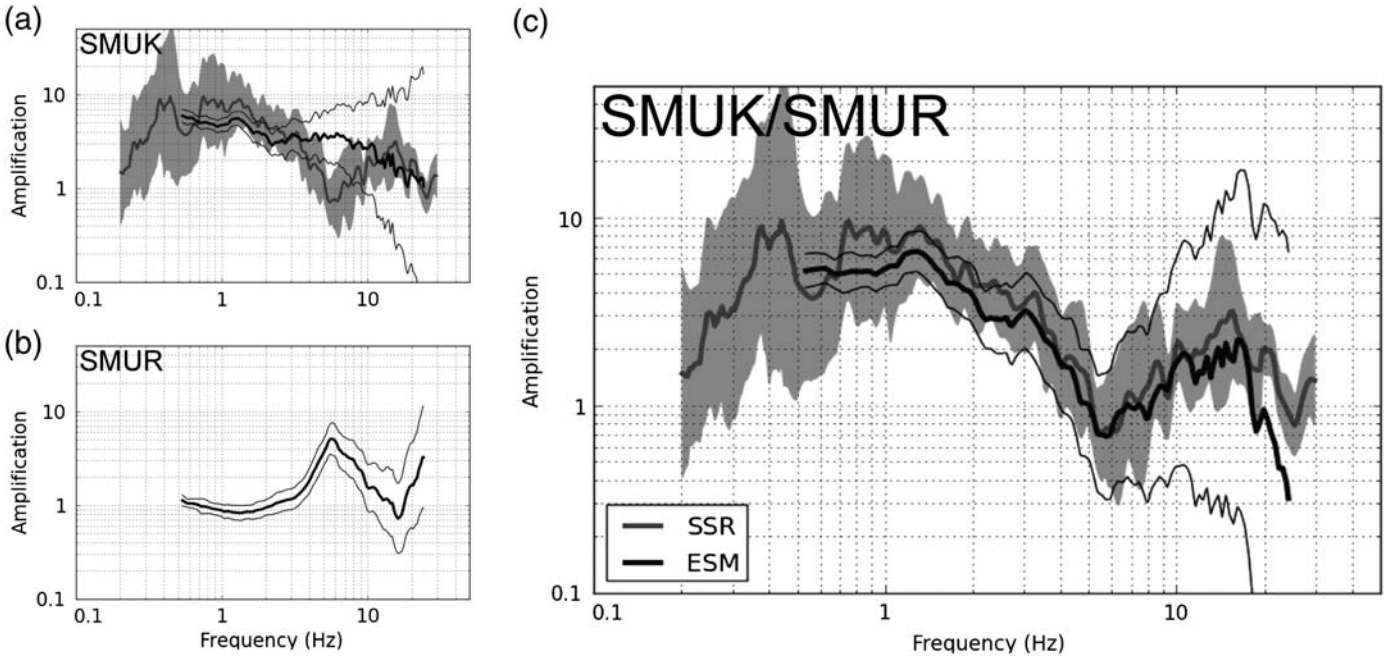

▲ **Figure 2.** (a) Standard spectral ratio SMUK/SMUR (gray) compared to ESM amplification at site SMUK (black). (b) ESM amplification of the reference site SMUR. (c) Comparison of the SSR SMUK/SMUR (gray) with the ratio of the ESM amplifications (black) between site and reference (SMUK/SMUR) finally selected for comparison.

compare amplification estimates, the SSR amplification functions were compared to the ratio of ESM amplifications at site and reference (Fig. 2). This approach completely negates the influence of the local reference site for the SSR and is used for all further comparisons.

Six pairs of stations are studied, the results of which are presented in Figure 3. The absolute amplification at the six non-reference sites is shown in the Ⓔ electronic supplement as Figure S1. The six target stations were chosen because they all have a nearby "local reference rock" site. Four of the pairs are located in the Rhone Valley (Valais, Switzerland), an area previously studied by Roten *et al.* (2006, 2008) and known to produce 2D amplification effects. One of the four pairs is located in Monthey (SMUK/SMUR), two in Sion (SIOM/SIOV and SIOO/SIOV) and one in Visp (SVIT/SVIO). In Sion, reference station SIOV is located on a hard rock outcrop located 1.5 km to the west of station SIOO and 700 m north of station SIOM. SIOM is located at the edge of a deep part of the basin, whereas SIOO is located in the center of the valley. In Visp, only a small number of recordings were available in the Rhone basin. Only station SVIT, located on a shallow alluvial fan adjacent to the valley, is presented here. Reference station SVIO is located on a rock outcrop, 350 m to the west of SVIT in the old town of Visp. A fifth pair of sites is located at the edge of the Rhine Valley (St. Gallen, Switzerland) in Buchs (SBUA2/SBUB), having a relatively distant hard rock reference at 3 km to the west. The last pair of sites (SLUW/SLUB) is located in Lucerne. Station SLUW is located on a lacustrine basin described in detail by Poggi *et al.* (2012). The reference station SLUB is located on a Molasse hill 1.5 km northwest from station SLUW. SLUB provides ESM amplification close to unity and is therefore assumed to be close to the reference rock for Switzerland used in this study.

Stations SIOM, SBUB, SBUA2, SLUB and SLUW were installed between 2010 and 2012 and characterized in the framework of the SSMNet renewal project (Michel *et al.*, 2012), whereas stations SVIO and SVIT were installed as part of the COGEAR project in 2010 (Fäh *et al.*, 2012). Therefore, the number of recorded events with sufficient signal-to-noise ratio is still limited, especially at low frequencies. Nevertheless, the overall agreement between ESM amplification and SSR is excellent, despite very different sites being presented, with amplifications ranging from close to unity in some frequency bands, up to 10. In some frequency ranges, the small features of the spectra are also reproduced. However, inconsistencies at low frequencies (below 1 Hz) can be noticed, where the ESM amplification is much smoother than the SSR amplification, leading to loss of resolution. One such example can be seen in the fundamental frequency of the Rhone basin at SIOO, which is 0.5 Hz. This is due to the fact that we use the multitaper algorithm to obtain smooth Fourier spectra for the ESM. Along with the duration-limited analysis signal this may lead to a loss of resolution at low frequencies. At high frequencies ($f > 10$ Hz), the mean ESM amplification ratio is again very close to the SSR, despite an obvious increase in uncertainty due to the sensitivity to the determination of $\Delta\kappa_j$.

COMPARISON OF EMPIRICAL SITE AMPLIFICATION WITH 1D SH-WAVE MODELING

The previous analysis showed that the ESM approach produces results consistent with those from SSR in the case in which

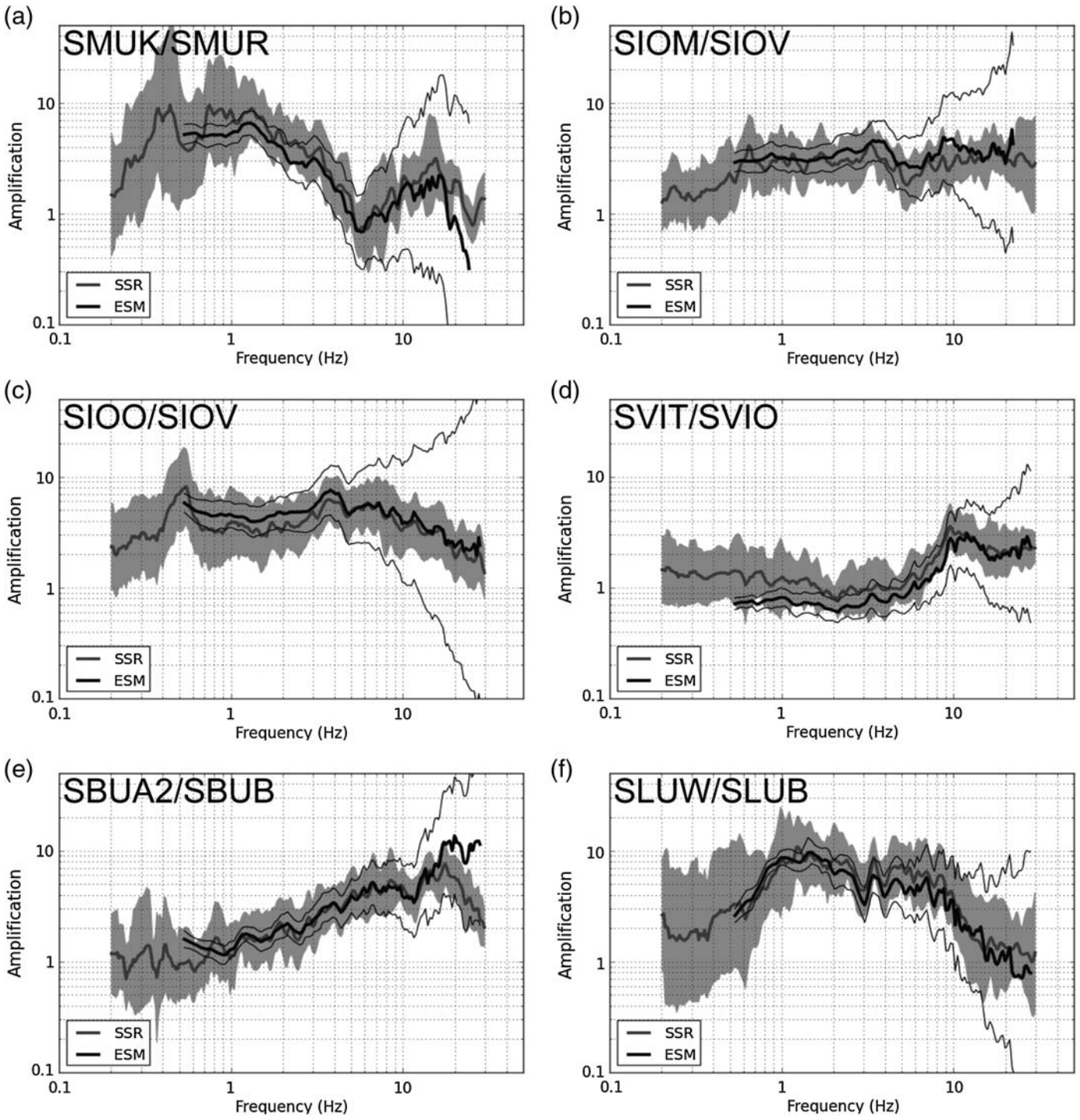

▲ **Figure 3.** Comparison of Standard Spectral Ratios (gray) with ratios of ESM amplifications (black) for six station pairs of SSMNet.

nearby reference sites existed. However, in contrast to the SSR approach, the application of the ESM approach is not only limited to such cases. In order to show the advantage of the spectral modeling technique over other commonly applied methods in site-response analysis, we compared the elastic ESM amplification functions with modeled one-dimensional, elastic SH-wave transfer functions (Knopoff, 1964) at several specific target sites of the SSMNet. The velocity profiles for these sites were obtained from surface-wave analysis of ambient vibration array recordings (Havenith *et al.*, 2007; Fäh *et al.*, 2009; Michel *et al.*, 2012). As mentioned, the ESM amplification always refers to a common rock reference velocity profile, which in the case of Switzerland has a gradient form with velocity increasing from around 1 to 3.2 km/s, as described in Poggi *et al.* (2011). In the case of an analytical 1D SH-amplification function, however, the reference is generally local. This can be based

on either real outcropping bedrock or the deep portion of the bedrock, virtually outcropped by removing the top sediment cover from the velocity profile. As with the SSR approach, comparing the SHTF and ESM approaches without accounting for the differences in the reference may result in large deviations.

In order to correct the SH transfer functions (with local reference) to the Swiss reference (target), we apply a method that is based on the use of the quarter-wavelength approach (Joyner *et al.*, 1981). In this method, a correction function is computed as the square root of the ratio between seismic impedances (Z) between the two references (local and target). Average seismic impedances are calculated using the quarter-wavelength method, which makes this parameter frequency dependent. The correction function is based on the original formulation by Joyner *et al.* (1981) and is given by

$$C(f) = \sqrt{\frac{Z^{\mathrm{Qwl}}_{\mathrm{Target}}(f)}{Z^{\mathrm{Qwl}}_{\mathrm{Local}}(f)}} = \sqrt{\frac{V^{\mathrm{Qwl}}_{S_{\mathrm{Target}}}(f)\rho^{\mathrm{Qwl}}_{\mathrm{Target}}(f)}{V^{\mathrm{Qwl}}_{S_{\mathrm{Local}}}(f)\rho^{\mathrm{Qwl}}_{\mathrm{Local}}(f)}}, \tag{5}$$

where V_S is the shear-wave velocity, ρ is density, and Qwl indicates averaging using the quarter-wavelength approach.

A simplification of equation (5) can be obtained through two considerations:

1. The difference in density has little impact in the final correction function; we can therefore neglect this parameter, assuming equal density between the two profiles.
2. For the transfer function modeling, the last layer of the discrete velocity profile is usually assumed as the reference. Therefore, being a layer of constant velocity, its quarter-wavelength expression will also be constant (frequency independent).

In this case equation (5) can be simplified to

$$C(f) = \sqrt{\frac{V^{\mathrm{Qwl}}_{S_{\mathrm{Target}}}(f)}{V_{S_{\mathrm{Local}}}}}, \tag{6}$$

where $V_{S_{\mathrm{Local}}}$ is the velocity of the local reference: the lowermost (base) layer of the local site's shear-wave velocity profile. The reference corrected amplification function $A^{\mathrm{Corr}}_{\mathrm{SH}}(f)$ can then be obtained by multiplication with the local correction function

$$A^{\mathrm{Corr}}_{\mathrm{SH}}(f) = C(f)A_{\mathrm{SH}}(f). \tag{7}$$

Figure 4 shows an example of correcting the analytical elastic SH amplification function with local reference at the station SCUG to the Swiss generic rock reference. The correction to the common Swiss reference pulls the high frequency part down, making it comparable with the ESM amplification determined in this study. The main advantage of this correction method is its simplicity, as it gives the possibility to correct existing amplification functions without recomputing the whole transfer function to the target reference. Such an approach, nevertheless, must be regarded as an approximation,

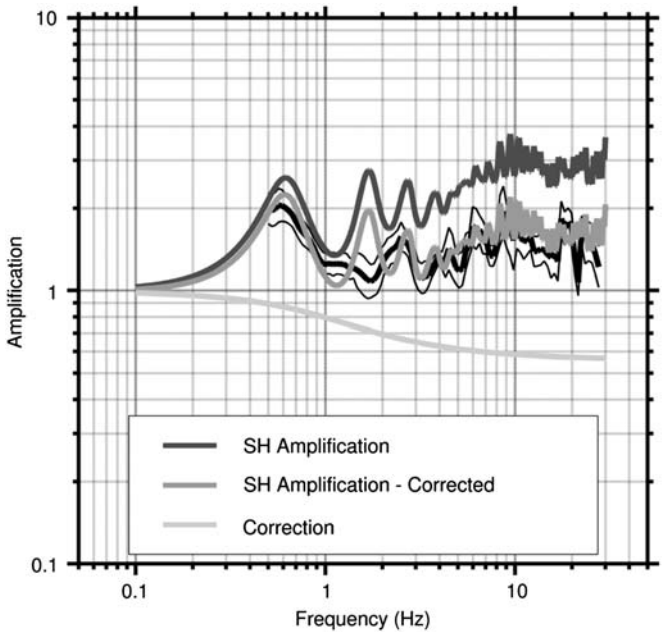

▲ **Figure 4.** Example of correcting the elastic amplification from *SH*-wave transfer function modeling at the SSMNet station SCUG to the common reference by applying the proposed correction function. Comparison with the ESM amplification function proposed in this paper (black).

producing a much smoother result than that expected from full modeling.

The comparison between elastic ESM amplification functions from the spectral fitting approach and the corrected analytical elastic solution from SH-transfer function computation has been carried out for six stations of the SSMNet (SYVP, SLTM, ZUR, OTTER, SEPFL, and SLUW). These sites represent a selection of sites within the strong-motion network for which a reliable assessment of the velocity structure is available (Havenith *et al.*, 2007; Fäh *et al.*, 2009; Michel *et al.*, 2012). The selection was made to highlight the diversity of available sites in addition to the limitations of 1D site characterization. In addition to the stations previously described, station OTTER is located in Basel on top of a deep sedimentary basin of the Rhine Graben; ZUR is located on top of a molasse hill in the city of Zurich; station SYVP is located on the deep lacustrine basin of lake Neuchâtel in the city center of Yverdon-les-Bains; SLTM2 is located in the narrow but deeply-filled alpine valley of the Linth, and SEPFL is located on shallow lacustrine sediments on the shore of lake Geneva in the École Polytechnique Fédérale de Lausanne campus. The results of these comparisons are presented in Figure 5. Due to the correction of the SH-amplification functions using equation (7), all the examples refer to the Swiss rock reference.

The match between the two types of amplification functions is good. In some cases (SYVP and SEPFL) even fine-scale features, such as the resonance peaks, are well represented in addition to the overall smooth shape. This indicates that the dimensioning of the velocity interfaces along the velocity

model is consistent with the observed amplification. In other cases, the 1D SH-modeled resonance behavior mismatches with the amplification obtained using the spectral inversion approach at high frequencies (e.g., SLTM2). This may be because of the poor resolution of the velocity profile at shallow depths leading to an incorrect SHTF at high frequency. The same can be observed at low frequencies, if the input velocity profile is not sufficiently constrained at relatively large depth (e.g., OTTER). Nevertheless, some mismatch can also be expected independent of the reliability of the velocity profile. At the station ZUR, for instance, the high frequency part mismatches. This may be due to a residual presence of attenuation in the elastic ESM amplification function; attenuation might not be entirely removed or, as in this case, may be overcorrected for in the spectral modeling due to trade-off between inverted parameters. A special comment is necessary for the station SLUW, which exhibits amplification factors up to 10 in all approaches. In the comparison of SSR with ESM amplifications,

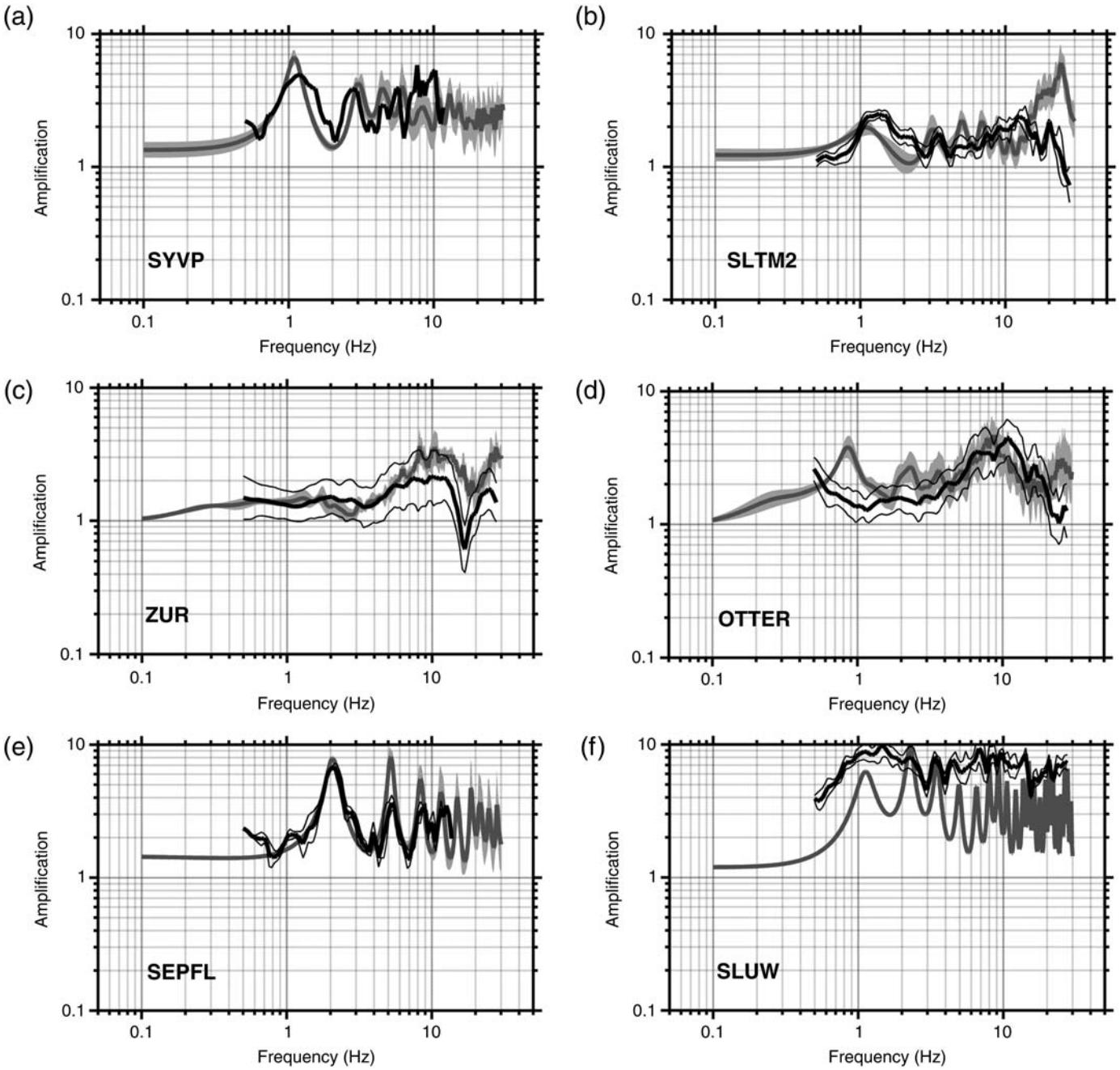

▲ **Figure 5.** Comparison of elastic ESM amplification functions from broadband spectral fitting (black line) and reference corrected elastic *SH*-wave transfer function modeling (in gray) at six test sites in Switzerland. Uncertainties are also shown, when available.

we observed an almost exact match, whereas in this case, a mismatch between ESM and SHTF amplification functions is induced by the presence of 2D/3D effects (e.g., Thompson *et al.*, 2009), which cannot be accounted for with simple 1D modeling.

COMPARISON OF EMPIRICAL SITE AMPLIFICATION WITH H/V RATIOS

The SDSNet is a broadband seismic network with installations typically on NEHERP rock or hard rock classes. Recordings of ambient noise from the continuous data stream were used to obtain single station H/V Fourier spectral ratios at all sites of the SDSNet. Recordings were taken over a duration of approximately one hour. Classical polarization analysis was then undertaken, following the approach detailed in Fäh *et al.* (2001). In order to avoid problems associated with the time variance of the noise field the ambient noise recordings are split into numerous 2048-sample (17-second) windows, each overlapping by 25%. With N as the number of windows, the geometrical average H/V, is then given by

$$\log\left[\frac{H}{V}(f)\right] = \frac{1}{N}\sum_{i=1}^{N}\log\left(\frac{\sqrt{H_{N,i}(f)H_{E,i}(f)}}{V_i(f)}\right). \quad (8)$$

To compare with the H/V function, the elastic ESM amplification function is reconstructed from the product of $a_j(f)$ and A_j, neglecting the attenuation term (Fig. 6). This is based on the assumption that the horizontal and vertical attenuation are comparable (Bethmann *et al.*, 2012). The best match between the shape of the H/V curve and ESM amplification is found at sites WEIN and WILA. However, a constant offset between H/V and elastic ESM amplification is observed for most stations. The most important source for the differences in shape is that amplification is simply not adequately represented by H/V spectral ratios, most pronounced by the constant offset. Peaks and troughs in the curves are related to the fundamental frequency of resonance of the surface layers, best seen at sites WEIN, WILA, ZUR, TORNY, and FLACH. This is thought to represent a combination of *S*-wave resonance and Rayleigh wave ellipticity (Poggi *et al.*, 2012), whereas in the case of the ESM, SSR, or SHTF, amplification is directly represented.

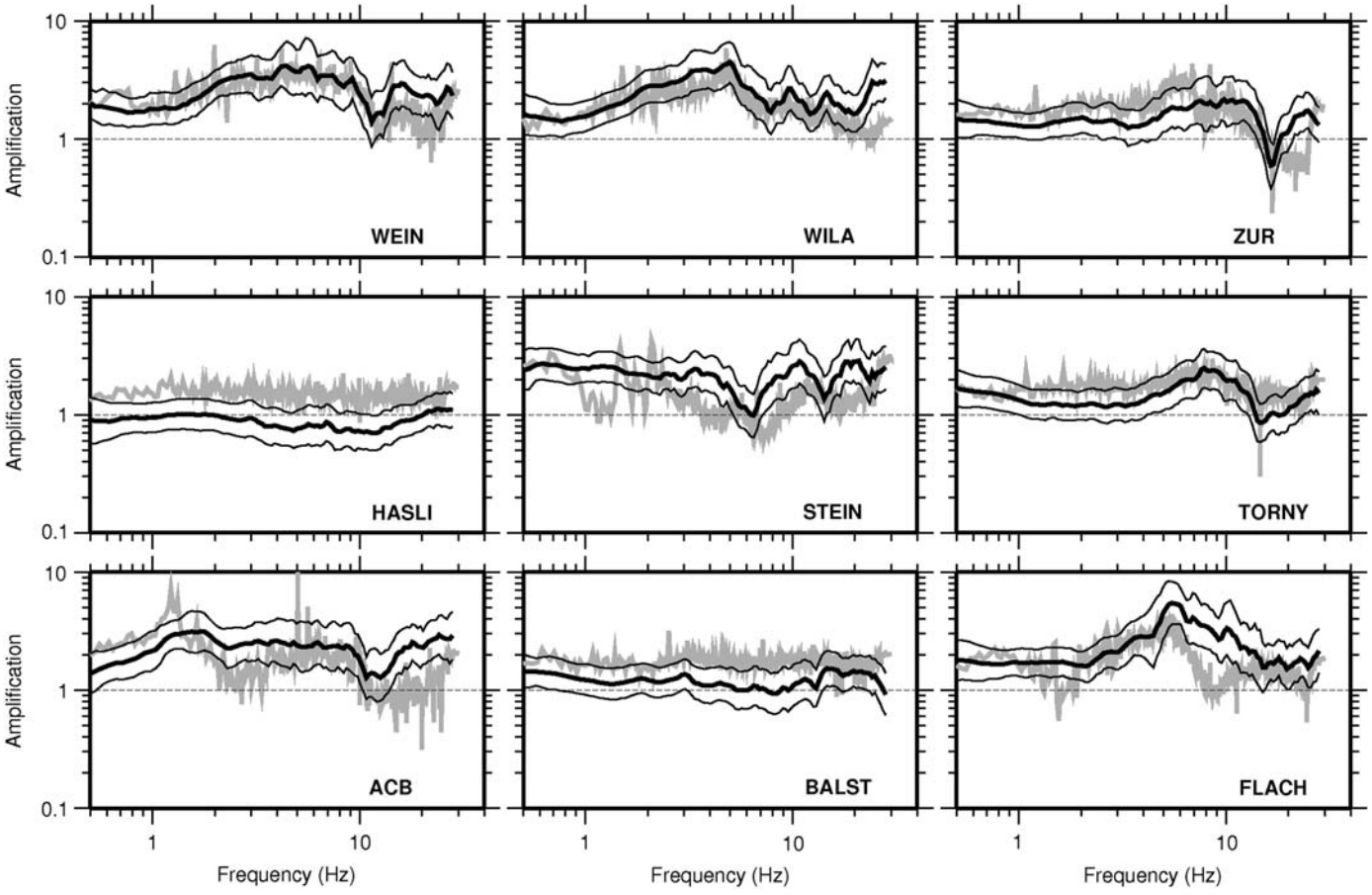

▲ **Figure 6.** H/V ratios for nine selected sites of the SDSNet compared with the elastic ESM amplification. The gray line shows the H/V derived from the ambient noise field using classical polarization analysis, the black line shows the elastic ESM amplification derived from earthquake recordings with corresponding standard deviation (thin black lines).

CONCLUSIONS

We presented and tested a method to determine elastic site response and corresponding local attenuation, referenced to a regional velocity profile. The method has a wide possibility of application, as the size of the recorded earthquakes only limits the frequency bandwidth of the recovered site amplification; the method can therefore be applied even in regions of low seismicity such as Switzerland. However, the method is equally applicable in seismically active areas of the world, where small earthquakes are abundant, and can be used to estimate the linear amplification phenomena to be expected in the case of larger, damaging events. The recovered site amplification using this method reflects the observed site amplification in that it includes focusing effects, resonance phenomena, and topographical effects. No separation of these individual features was undertaken, however, comparison with 1D-SH modeling suggests that 2D and 3D effects may have a significant impact on local amplification, especially in Alpine valleys.

The proposed spectral fitting method was tested against standard methods for estimation of site response. The match with site-to-reference spectral ratios was excellent as long as we compared the ratio of amplifications in order to account for the fact that the SSR method may not have unitary reference amplification. Smoothing issues of the presented method at low frequencies were highlighted, however, and are due to the use of the multi-taper approach to compute the Fourier transform in addition to the duration-limited analysis signals. Unfortunately, there exists a trade-off between signal isolation and SNR maximization with the robustness of low-frequency estimation. In order to compare with a 1D modeling method, we corrected SH-transfer model amplifications to a common reference using the quarter-wavelength approximation. This is important because 1D SH-modeling typically has a local reference, usually the bedrock layer beneath the site. After correction, the two methods showed good agreement, in some cases even including fine-scale features such as resonance peaks.

Comparison of amplification from spectral fitting with estimations of the H/V ratio found an agreement in shape, although significant differences were present between amplitudes at most sites. The H/V analysis undertaken disagrees with the conclusions of Nakamura (1989), who suggested that the use of H/V ratios can approximate site response. While the approach does provide a reasonable first-order estimate of the shape of the amplification related to resonance behavior (i.e., the location of resonance peaks), the amplitudes obtained from H/V measurements are not representative of ground-motion amplification. One aspect to consider is that the H/V function rarely indicates deamplification, which is possible when amplification is considered with respect to a common reference. We conclude, therefore, that the H/V ratio should not be used to predict amplification.

Overall, the method presented here to determine elastic amplification functions for sites within a seismic network offers a useful tool for network operation and hazard assessment. The agreement with existing approaches showed the validity of the method in specific cases for which detailed site information was available or a reference site with negligible amplification was nearby. The proposed method is extended without loss of generality to all sites in the network, regardless of whether velocity information or other site characterization information exists. In fact, the method can be useful in helping to characterize sites, for example, by providing information on resonance phenomena, indicating strong contrasts of impedance at depth or highlighting particularly strong or weak local attenuation. Application to the hazard analysis of specific sites such as sensitive facilities or unstable rock slopes (e.g., Burjanek *et al.*, 2012) can be considered through the installation of a strong-motion station for a limited period of time depending on the level of seismicity.

ACKNOWLEDGMENTS

This work was funded in part by the Swiss Federal Nuclear Safety Inspectorate (ENSI) and in part by the project for the Renewal of the Swiss Strong Motion Network (SSMNet), which is supported by the Federal Office for the Environment (FOEN), the Federal Roads Office (FEDRO), ENSI, Swiss Federal Railways (SBB), Schweizerischer Pool für Erdbebendeckung and ETH Zurich. The data used for this study are freely available online at arclink.ethz.ch. We thank Laurie Baise and Editor in Chief Jonathan Lees for their review of this manuscript.

REFERENCES

Abrahamson, N., and W. Silva (2008). Summary of the Abrahamson & Silva NGA ground-motion relations, *Earthq. Spectra* **24,** 67–97.

Akkar, S., and J. J. Bommer (2010). Empirical equations for the prediction of PGA, PGV, and spectral accelerations in Europe, the Mediterranean region, and the Middle East, *Seismol. Res. Lett.* **81,** 195–206.

Al Atik, L., N. Abrahamson, J. J. Bommer, F. Scherbaum, F. Cotton, and N. Kuehn (2010). The variability of ground-motion prediction models and its components, *Seismol. Res. Lett.* **81,** 794–801.

Anderson, J. G., and S. E. Hough (1984). A model for the shape of the fourier amplitude spectrum of acceleration at high-frequencies, *Bull. Seismol. Soc. Am.* **74,** 1969–1993.

Atkinson, G. M. (2006). Single-station sigma, *Bull. Seismol. Soc. Am.* **96,** 446–455.

Atkinson, G. M., and D. M. Boore (2006). Earthquake ground-motion prediction equations for eastern North America, *Bull. Seismol. Soc. Am.* **96,** 2181–2205.

Atkinson, G. M., and R. F. Mereu (1992). The shape of ground motion attenuation curves in southeastern Canada, *Bull. Seismol. Soc. Am.* **82,** 2014–2031.

Bethmann, F., N. Deichmann, and P. M. Mai (2012). Seismic wave attenuation from borehole and surface records in the top 2.5 km beneath the city of Basel, Switzerland, *Geophys. J. Int.* **190,** 1257–1270.

Bonnefoy-Claudet, S., C. Cornou, P. Y. Bard, F. Cotton, P. Moczo, J. Kristek, and D. Fah (2006). H/V ratio: A tool for site effects evaluation. Results from 1-D noise simulations, *Geophys. J. Int.* **167,** 827–837.

Boore, D. M. (2004). Can site response be predicted? *J. Earthq. Eng.* **8,** 1–41.

Borcherdt, R. D. (1970). Effects of local geology on ground motion near San Francisco Bay, *Bull. Seismol. Soc. Am.* **60,** 29–61.

Brune, J. N. (1970). Tectonic stress and spectra of seismic shear waves from earthquakes, *J. Geophys. Res.* **75,** 4997–5009.
Brune, J. N. (1971). Correction, *J. Geophys. Res.* **76,** 5002.
Building Seismic Safety Council (BSSC) (2003). *The 2003 NEHRP Recommended Provisions for New Buildings and Other Structures (FEMA 450), Part 1: Provisions*, Federal Emergency Management Agency, Washington, D.C., 308 pp.
Burjanek, J., J. R. Moore, F. X. Y. Molina, and D. Fäh (2012). Instrumental evidence of normal mode rock slope vibration, *Geophys. J. Int.* **188,** 559–569.
Clinton, J., C. Cauzzi, D. Fäh, C. Michel, P. Zweifel, M. Olivieri, G. Cua, F. Haslinger, and D. Giardini (2011). The current state of strong motion monitoring in Switzerland, in *Earthquake Data in Engineering Seismology*, S. Akkar, P. Gülkan, and T. van Eck (Editors), Springer, Netherlands, 219–233, doi: 10.1007/978-94-007-0152-6_15.
Deichmann, N., J. Clinton, S. Husen, B. Edwards, F. Haslinger, D. Fäh, D. Giardini, P. Kästli, U. Kradolfer, and I. Marschall (2010). Earthquakes in Switzerland and surrounding regions during 2009, *Swiss J. Geosci.* **103,** 535–549.
Edwards, B., and D. Fäh (2013). A stochastic ground-motion model for Switzerland, *Bull. Seismol. Soc. Am.* **103,** 78–98.
Edwards, B., B. Allmann, D. Fäh, and J. Clinton (2010). Automatic computation of moment magnitudes for small earthquakes and the scaling of local to moment magnitude, *Geophys. J. Int.* **183,** 407–420.
Edwards, B., D. Fäh, and D. Giardini (2011). Attenuation of seismic shear wave energy in Switzerland, *Geophys. J. Int.* **185,** 967–984.
Edwards, B., A. Rietbrock, J. J. Bommer, and B. Baptie (2008). The acquisition of source, path, and site effects from microearthquake recordings using Q tomography: Application to the United Kingdom, *Bull. Seismol. Soc. Am.* **98,** 1915–1935.
Fäh, D., S. Fritsche, V. Poggi, G. Gassner-Stamm, P. Kästli, J. Burjanek, P. Zweifel, S. Barman, J. Clinton, and L. Keller (2009). Determination of site information for seismic stations in Switzerland, *Swiss Seismological Service Tech. Rept.: SED/PRP/R/004/20090831 for the swissnuclear PEGASOS Refinement Project*.
Fäh, D., F. Kind, and D. Giardini (2001). A theoretical investigation of average H/V ratios, *Geophys. J. Int.* **145,** 535–549.
Fäh, D., F. Kind, and D. Giardini (2003). Inversion of local *S*-wave velocity structures from average H/V ratios, and their use for the estimation of site-effects, *J. Seismol.* **7,** 449–467.
Fäh, D., J. R. Moore, J. Burjanek, I. Iosifescu, D. Dalguer, F. Dupray, C. Michel, J. Woessner, A. Villiger, and J. Laue (2012). Coupled seismogenic geohazards in alpine regions, *Bollettino Di Geofisica Teorica Ed Applicata* **53,** 485–508.
Fäh, D., G. Stamm, and H. B. Havenith (2008). Analysis of three-component ambient vibration array measurements, *Geophys. J. Int.* **172,** 199–213.
Field, E. H., and K. H. Jacob (1995). A comparison and test of various site-response estimation techniques, including three that are not reference-site dependent, *Bull. Seismol. Soc. Am.* **85,** 1127–1143.
Havenith, H. B., D. Fäh, U. Polom, and A. Roulle (2007). *S*-wave velocity measurements applied to the seismic microzonation of Basel, Upper Rhine Graben, *Geophys. J. Int.* **170,** 346–358.
Joyner, W. B., R. E. Warrick, and T. E. Fumal (1981). The effect of quaternary alluvium on strong ground motion in the Coyote Lake, California, earthquake of 1979, *Bull. Seismol. Soc. Am.* **71,** 1333–1349.
Knopoff, L. (1964). A matrix method for elastic wave problems, *Bull. Seismol. Soc. Am.* **54,** 431–438.
Konno, K., and T. Ohmachi (1998). Ground-motion characteristics estimated from spectral ratio between horizontal and vertical components of microtremor, *Bull. Seismol. Soc. Am.* **88,** 228–241.
Michel, C., C. Cauzzi, D. Fäh, J. Clinton, P. Zweifel, and P. Kästli (2012). The Swiss strong-motion network: High-quality strong-motion monitoring in a region of low-to-moderate seismicity, in *Proc. 15th World Conference on Earthquake Engineering (15 WCEE)*, Lisbon, Portugal, 24–28 September 2012, paper no. 1470.
Nakamura, Y. (1989). A method for dynamic characteristics estimation of subsurface using microtremor on the ground surface, *Railway Technical Research Institute, Quarterly Reports* **30,** 25–33.
Poggi, V., and D. Fäh (2010). Estimating Rayleigh wave particle motion from three-component array analysis of ambient vibrations, *Geophys. J. Int.* **180,** 251–267.
Poggi, V., B. Edwards, and D. Fäh (2011). Derivation of a reference shear-wave velocity model from empirical site amplification, *Bull. Seismol. Soc. Am.* **101,** 258–274.
Poggi, V., D. Fäh, J. Burjanek, and D. Giardini (2012). The use of Rayleigh-wave ellipticity for site-specific hazard assessment and microzonation: Application to the city of Lucerne, Switzerland, *Geophys. J. Int.* **188,** 1154–1172.
Roten, D., D. Fäh, C. Cornou, and D. Giardini (2006). Two-dimensional resonances in Alpine valleys identified from ambient vibration wavefields, *Geophys. J. Int.* **165,** 889–905.
Roten, D., D. Fäh, K. B. Olsen, and D. Giardini (2008). A comparison of observed and simulated site response in the Rhone valley, *Geophys. J. Int.* **173,** 958–978.
Scherbaum, F., K. G. Hinzen, M. Ohrnberger, and R. B. Herrmann (2003). Determination of shallow shear wave velocity profiles in the Cologne, Germany area using ambient vibrations, *Geophys. J. Int.* **152,** 597–612.
Steidl, J. H., A. G. Tumarkin, and R. J. Archuleta (1996). What is a reference site? *Bull. Seismol. Soc. Am.* **86,** 1733–1748.
Thompson, E. M., L. G. Baise, R. E. Kayen, and B. B. Guzina (2009). Impediments to predicting site response: Seismic property estimation and modeling simplifications, *Bull. Seismol. Soc. Am.* **99,** 2927–2949.
Thompson, E. M., L. G. Baise, Y. Tanaka, and R. E. Kayen (2012). A taxonomy of site response complexity, *Soil Dynam. Earthq. Eng.* **41,** 32–43.

Benjamin Edwards
Clotaire Michel
Valerio Poggi
Donat Fäh
Swiss Seismological Service
ETH Zürich, Sonneggstrasse, 5
8092 Zürich, Switzerland
edwards@sed.ethz.ch